VLF-EM anomalies simulation by underground line sources of alternating current

Edson E. S. Sampaio, IGEO-CPGG/UFBA

Abstract

We have determined the variation of the anomalous magnetic field components due to the scattering of very low frequency electromagnetic (VLF-EM) fields by an underground planar conductor. We have modeled the anomalous conductor by a set of electromagnetic line sources and have taken into account the variation with depth of both the phase and the attenuation of the electromagnetic energy. We have analysed and compared the results between the field components and the parameters of the related polarization ellipsis.

Introduction

Very low frequency electromagnetic (VLF-EM) is a man-made non-controlled source electromagnetic geophysical method for near-surface exploration. It is specially suited for the determination of dipping shear zones that present a contrast of conductivity with the bedrock. McNeill and Labson (1991) present a detailed description of it for geological mapping. Karous and Hjelt (1983) developed a modeling for this method, simulating underground conductors by a distribution of line sources with direct electrical currents along a constant depth and Kaikkonen (1979) developed a more elaborated VLF numerical modeling by employing finite element analysis.

In this paper, we employ line sources with alternate electric currents, distributed at any point of a vertical plane, to model underground conductors. As such, it takes into account the spatial variation of both the phase and the amplitude of any component of the energy and doesn't limit the distribution of the line sources to a horizontal plane. Our development follows from the basic formulation of the field of an EM line source of Ward and Hohmann (1988) and the description of the parameters of the polarization ellipsis given by Smith and Ward (1974).

The line source and its related earth model

According to Ward and Hohmann (1988), the frequency domain magnetic field, $\mathbf{H}$, due to a harmonic line source along the y direction varies as follows:

$$\mathbf{H}(x,z) = \frac{I}{2\pi} i\kappa\rho\, K_1 \left(\frac{z-\zeta}{\rho^2}\mathbf{u}_x - \frac{x-\xi}{\rho^2}\mathbf{u}_z \right). \qquad (1)$$

In Equation 1: (x,z) are the coordinates of the observation point; (ξ,ζ) are the coordinates of the line source; $\rho = \sqrt{(x-\xi)^2+(z-\zeta)^2}$ is the source-receiver distance; I is the current of the line source; K_1 is the modified Bessel function of second kind, order 1, and argument $i\kappa\rho$; $i = \sqrt{-1}$; the wave number $\kappa = \sqrt{\mu\varepsilon\omega^2 - i\mu\sigma\omega}$, $\Im(\kappa) < 0$; μ is the magnetic permeability; ε is the dielectric permittivity; σ is the conductivity; and ω is the frequency.

We propose to model the line source by a prism with an infinitely long horizontal axis along the y axis and a vertical rectangular section $\Delta\xi\,\Delta\zeta$, in which $I = J\Delta\xi\,\Delta\zeta$, J being the current density.

We will assume, initially, that N underground line sources, $\zeta > 0$, cause a secondary magnetic field measured at stations along a profile, $z = 0$, $x = x_l$, $l = 1,2,\ldots,L$, and that the stations have a constant separation Δx. So, we may split Equation 1 into the following two equations:

$$H_z(x_l,0) = -\frac{\Delta\xi\,\Delta\zeta}{2\pi}\sum_{n=1}^{N} J(\xi_n,\zeta_n)\, i\kappa\rho_{ln} K_1 \frac{x_l-\xi_n}{\rho_{ln}^2}, \qquad (2)$$

$$H_x(x_l,0) = -\frac{\Delta\xi\,\Delta\zeta}{2\pi}\sum_{n=1}^{N} J(\xi_n,\zeta_n)\, i\kappa\rho_{ln} K_1 \frac{\zeta_m}{\rho_{ln}^2}, \qquad (3)$$

Then, let us associate those line sources to 2-D regions of the subsurface and confer to each of them an anomalous conductivity value, $\sigma_a(\xi_n,\zeta_n) \gg \sigma$. Under those circumstances, we may infer that a plane-wave VLF electromagnetic field yields a current density $J(\xi_n,\zeta_n)$ along each line source via its y-component electric field, $E_{yp}(\zeta) = E_{y0}\, e^{-i\kappa\zeta}$. Therefore:

$$\begin{aligned} J(\xi_n,\zeta_n) &= \sigma_a(\xi_n,\zeta_n) E_{yp}(\zeta_n) \\ &= -\sigma_a(\xi_n,\zeta_n)\frac{\omega\mu}{\kappa} H_{x0} e^{-i\kappa\zeta_n}. \end{aligned} \qquad (4)$$

In Equation 4, E_{y0} and H_{x0} are, respectively, the values of the y-oriented electric and x-oriented magnetic components of the plane-wave VLF field at $z = 0$. Notice that, if $H_{x0} > 0$ then $E_{y0} < 0$ and $J(\xi_n,\zeta_n) < 0$.

We assume, for all practical purposes, that the current vanishes outside the anomalous conductivity regions, because the background conductivity is much smaller than the anomalous conductivity.

Therefore, we may rewrite Equations 2 and 3 as

$$H_z(x_l,0) = \overline{E}_0 \sum_{n=1}^{N} e^{-i\kappa\zeta_n}\sigma_a(\xi_n,\zeta_n)\, i\kappa\rho_{ln} K_1 \frac{x_l-\xi_n}{\rho_{ln}^2}, \qquad (5)$$

$$H_x(x_l,0) = \overline{E}_0 \sum_{n=1}^{N} e^{-i\kappa\zeta_n}\sigma_a(\xi_n,\zeta_n)\, i\kappa\rho_{ln} K_1 \frac{\zeta_n}{\rho_{ln}^2}, \qquad (6)$$

$$\overline{E}_0 = \frac{\omega\mu\Delta\xi\,\Delta\zeta H_p \cos(\beta)}{2\pi\kappa}, \qquad (7)$$

$H_p > 0$ is the magnitude of the horizontal vector that represents the value of the plane wave magnetic field at $z = 0$ and β is the angle between this vector and the x axis. We assume that $0 \le \beta < \pi/2$, what implies that $H_p \ge H_{x0} > 0$.

Linear inversion of the conductivity values of the anomalous regions

We can employ the values of the real and the imaginary parts of both $H_z(x_l,0)$ and $H_x(x_l,0)$ given in Equations 5 and 6 to solve the N real values of $\sigma_a(\xi_n,\zeta_n)$ as long as $4L \geq N$.

For this purpose let us express Equations 5 and 6 jointly in matrix form as:

$$\overline{H}_s = A_{s\times n}\cdot\Sigma_n. \tag{8}$$

In Equation 8:

$$\overline{H}_s = \begin{cases} \Re\left(\frac{H_z}{H_p}\right), & s=1,\ldots,L \\ \Im\left(\frac{H_z}{H_p}\right), & s=L+1,\ldots,2L \\ \Re\left(\frac{H_x}{H_p}\right), & s=2L+1,\ldots,3L \\ \Im\left(\frac{H_x}{H_p}\right), & s=3L+1,\ldots,4L \end{cases} \tag{9}$$

$$A_{s\times n} = \begin{cases} \Re\left(\frac{\overline{E}_0}{H_p}e^{-i\kappa\zeta_n}i\kappa\rho\,K_1\frac{x_l-\xi_n}{\rho^2}\right), & s=1,\ldots,L, \\ \Im\left(\frac{\overline{E}_0}{H_p}e^{-i\kappa\zeta_n}i\kappa\rho\,K_1\frac{x_l-\xi_n}{\rho^2}\right), & s=L+1,\ldots,2L, \\ \Re\left(\frac{\overline{E}_0}{H_p}e^{-i\kappa\zeta_n}i\kappa\rho\,K_1\frac{\zeta_n}{\rho^2}\right), & s=2L+1,\ldots,3L, \\ \Im\left(\frac{\overline{E}_0}{H_p}e^{-i\kappa\zeta_n}i\kappa\rho\,K_1\frac{\zeta_n}{\rho^2}\right), & s=3L+1,\ldots,4L, \end{cases} \tag{10}$$

$$\Sigma_n = \sigma_a(\xi_n,\zeta_n), \tag{11}$$

$n=1,\ldots,N$. Equation 8 is a linear equation in the N values of the anomalous conductivity. A well known solution of it is:

$$\Sigma_n = \left(A^T_{n\times s}\cdot A_{s\times n}\right)^{-1}\left(A^T_{n\times s}\cdot\overline{H}_s\right). \tag{12}$$

It may be possible to solve the N real values of $\sigma_a(\xi_n,\zeta_n)$ even if the condition $4L \geq N$ doesn't hold. For this underdetermined situation, it would be necessary to employ a procedure similar to that of Safon et al (1977), who applied linear programming to the inverse gravity problem. The requirements of this EM inverse modeling, equivalent to the gravity problem, are that all $\sigma_a(\xi_n,\zeta_n) > 0$ and to know the total anomalous current,

$$I_t = \sum_{n=1}^{N} J(\xi_n,\zeta_n)\Delta\xi\,\Delta\zeta. \tag{13}$$

We substitute $J(\xi_n,\zeta_n)$ in Equation 13 for the right-hand side of Equation 4 and the integral formula of Maxwell's equation, related to Ampère's law, implies that

$$\sum_{l=1}^{L} H_x(x_l,0)\Delta\xi = I_t. \tag{14}$$

Parameters of the polarization ellipsis

Usually, the VLF-EM data are not the magnetic field components themselves but rather the tilt angle of the major axis, θ_v, and the ellipticity, ε_v, of a vertical polarization ellipsis of the magnetic field or the related parameters of a horizontal polarization ellipsis: θ_h and ε_h. Based on developments by Smith and Ward (1974), McNeill and Labson (1991) shows that, as long as the ratio between the vertical and the horizontal components of the magnetic field is much smaller than one, the expressions for those parameters are approximately as follows:

$$\tan(2\theta_v) \approx 2\,\Re\left(\frac{H_z}{H_p\cos(\beta)+H_x}\right), \tag{15}$$

$$\varepsilon_v \approx \Im\left(\frac{H_z}{H_x}\right). \tag{16}$$

If these approximations hold, we could adopt a procedure similar to that of Equation 12 to model the values of σ_a by employing the measured values of the parameters of both the vertical and the horizontal polarization ellipsis. Notice that, for the horizontal ellipsis, it would be necessary to substitute H_z by $H_{y0} = H_p\sin(\beta)$ in Equations 15 and 16.

Results and Discussion

We will now employ Equations 5 and 6 to compute, respectively, $H_z(x_l,0)/H_p$ and $H_x(x_l,0)/H_p$ in the simulation of an anomalous region by line sources. We will assume that $\beta = \pi/6$ rd and the frequency $f = 10^4$ Hz for the primary VLF-EM field and that $\mu = 4\pi\times10^{-7}$ henry/m and $\sigma = 10^{-3}$ siemens/m for the background medium. Under these conditions, $\kappa \approx \sqrt{-i\mu\sigma\omega}\,\mathrm{m}^{-1}$, $\Im(\kappa) < 0$.

Let us simulate a shear zone with a constante value of σ_a, dipping about 45°, and with depths to the top and bottom respectively equal to 5 m and 45 m by $N = 8$ line sources such that: $(\xi_n = -17.5+5(n-1), \zeta_n = 7.5+5(n-1))$, $n = 1,2,\ldots,8$. In this case, $\Delta\xi = 10$ m and $\Delta\zeta = 5$ m. Recall that, ξ_n and ζ_n represent the coordinates of the center of the eight rectangles.

Figures 1, 2, 3, 4, 5, and 6 show the variation of the magnetic field components for this shear zone model for given values of σ_a. In Figures 2, 4, and 6, we have added to the value of $\Re(H_x(x_l,0)/H_p)$ the value of $H_{x0}/H_p = \cos(\beta)$.

All the curves are asymmetric, what reflects the dip of the shear zone to the right of the graphics. The H_z curves comply with the linear dependence of the functions with σ_a. The same happens with the imaginary part of H_x, but not with its real part, because of the contribution of the primary VLF-EM field to it.

The minimum values of the H_z curves are sharp, while their maximum values are smooth. This happens because the minimum values occur updip and consequently closer to the top of the shear zone. Also, the cross-overs occur in the vicinity of the top of the shear zone, because of the decreasing contribution of the deeper parts of it. For the same reason, the peak values of the H_x curves occur updip and they present a less steep decay in the downdip direction.

For $\sigma_a \leq 0.01$ S/m, $|H_z|$ is equal or less than 10 % of $|H_x|$. However, for $\sigma_a \geq 0.1$ S/m, $|H_z|$ excceeds 25 % of $|H_x|$. Therefore, the approximation defined by Equations 15 and 16 may hold only for shear zones that are slightly more conductive than the bedrock. Furthermore, for the horizontal ellipsis the approximation also requires that $\beta < \pi/6$ rd.

Conclusion

We have simulated underground conductivity anomalies by a distribution of line sources carrying alternating current.

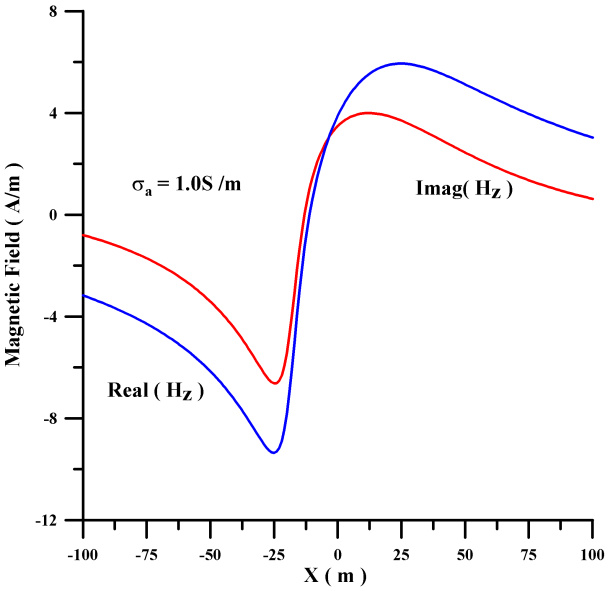

Figure 1: Variation of the real and imaginary parts of the vertical component of the magnetic field for a shear zone dipping about 45° and for $\sigma_a = 1$ S/m. The center of the top of the shear zone is at $(\xi = -17.5, \zeta = 5)$ and the center of the bottom of the shear zone is at $(\xi = 17.5, \zeta = 45)$.

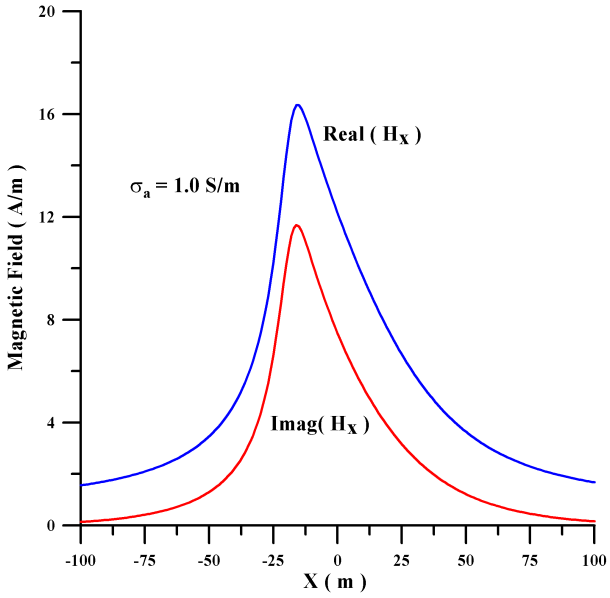

Figure 2: Variation of the real and imaginary parts of the horizontal component of the magnetic field for a shear zone dipping about 45° and for $\sigma_a = 1$ S/m. The center of the top of the shear zone is at $(\xi = -17.5, \zeta = 5)$ and the center of the bottom of the shear zone is at $(\xi = 17.5, \zeta = 45)$.

So, we have shown how to compute the magnetic field components that result from the scattering of a VLF-EM plane wave field by those anomalies. We also demonstrated that, for this particular model, the solution for the anomalous conductivity values results from a linear inverse modeling procedure.

These results are important for application in near-surface geophysical exploration for geological mapping of shear zones with the VLF-EM method. The present result consists of an improvement of the generalized Fraser filter because of two reasons: (1) it takes int account the variation with depth of the phase and amplitude of both the primary and the scattered field; (2) the distribution of line sources is not limited to a constant depth level.

VLF-EM surveys should measure the magnetic field components rather than the parameters of the related polarization ellipsis. This would assure the linearity of the inverse modeling of the conductivity values. Therefore, it would improve the interpretation of the geological features.

References

Kaikkonen, P., 1979, Numerical VLF modeling: Geophysical Prospecting, Vol. 27, p815-834.

Karous, M. and Hjelt, S. E., 1983, Linear filtering of VLF dip-angle measurements: Geophysical Prospecting, Vol. 31, p782-794.

McNeill J.D. and Labson V.F., 1991. Geological mapping using VLF radio fields, in M.N. Nabighian, ed. Electromagnetic Methods in Applied Geophysics, chapter 7, part B, volume 2, Application: SEG Investigation in Geophysics, no. 3, p521-640.

Safon, C. Vasseur, G. and Cuer, M., 1977, Some applications of linear programming to the inverse gravity problem: Geophysics, Vol. 42, p1215-1229.

Smith, B.,D. and Ward, S.,H., 1974, On the computation of polarization ellipse parameters: Geophysics, Vol. 39, p867-869.

Ward, S.,H. and Hohmann, G.,W., 1988, Electromagnetic theory for geophysical application, in M.N. Nabighian, ed. Electromagnetic Methods in Applied Geophysics, chapter 4, volume 1, Theory: SEG Investigation in Geophysics, no. 3, p131-311.

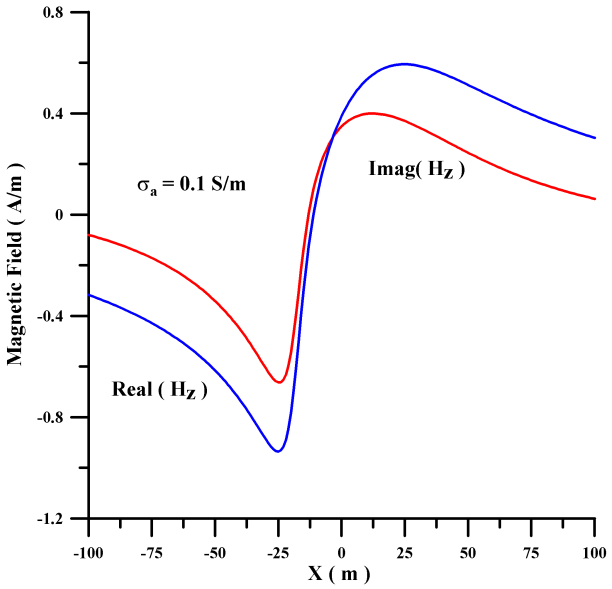

Figure 3: Variation of the real and imaginary parts of the vertical component of the magnetic field for a shear zone dipping about 45° and for $\sigma_a = 0.1$ S/m. The center of the top of the shear zone is at $(\xi = -17.5, \zeta = 5)$ and the center of the bottom of the shear zone is at $(\xi = 17.5, \zeta = 45)$.

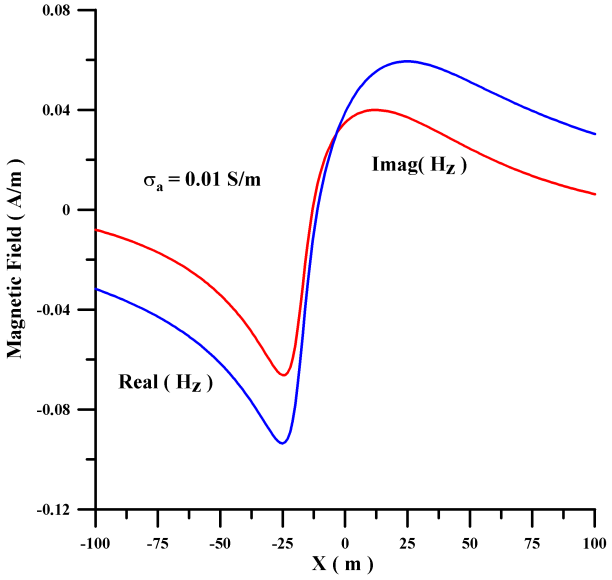

Figure 5: Variation of the real and imaginary parts of the vertical component of the magnetic field for a shear zone dipping about 45° and for $\sigma_a = 0.01$ S/m. The center of the top of the shear zone is at $(\xi = -17.5, \zeta = 5)$ and the center of the bottom of the shear zone is at $(\xi = 17.5, \zeta = 45)$.

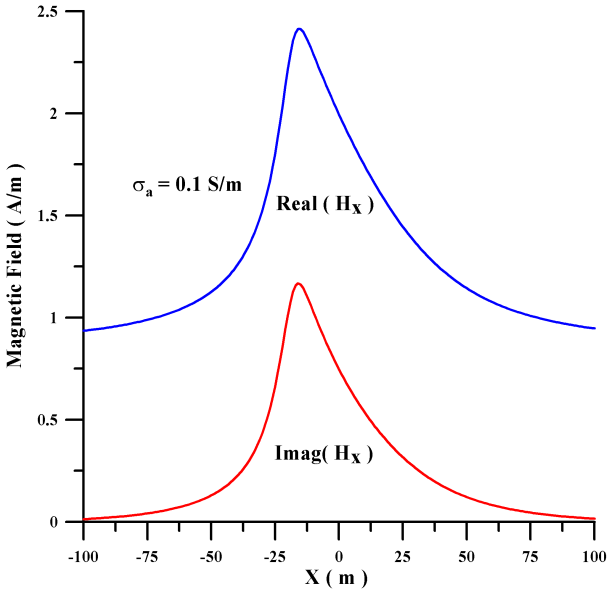

Figure 4: Variation of the real and imaginary parts of the horizontal component of the magnetic field for a shear zone dipping about 45° and for $\sigma_a = 0.1$ S/m. The center of the top of the shear zone is at $(\xi = -17.5, \zeta = 5)$ and the center of the bottom of the shear zone is at $(\xi = 17.5, \zeta = 45)$.

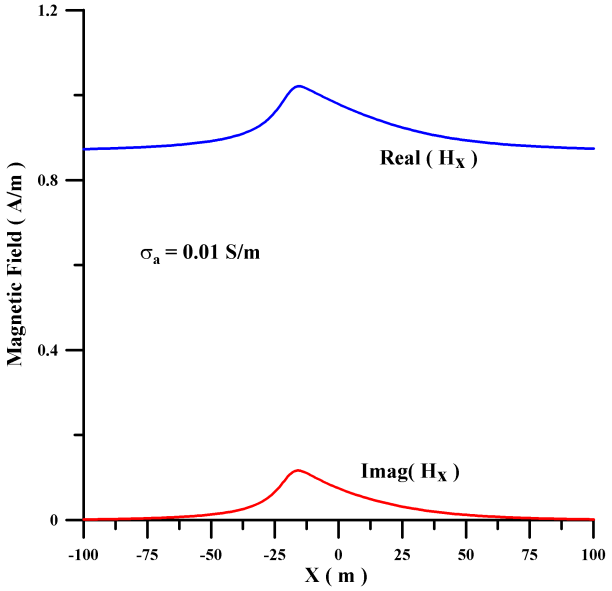

Figure 6: Variation of the real and imaginary parts of the horizontal component of the magnetic field for a shear zone dipping about 45° and for $\sigma_a = 0.01$ S/m. The center of the top of the shear zone is at $(\xi = -17.5, \zeta = 5)$ and the center of the bottom of the shear zone is at $(\xi = 17.5, \zeta = 45)$.